

# Band gap and stability in the ternary intermetallic compounds NiSnM (M = Ti, Zr, Hf): A first principles study

Serdar Ögüt and Karin M. Rabe

*Yale University, Physics Department*

*P. O. Box 208120, New Haven, Connecticut, 06520-8120*

(October 25, 2018)

## Abstract

The structural stability and electronic properties of the ternary intermetallic compounds NiSnM (M = Ti, Zr, Hf) and the closely related Heusler compounds Ni<sub>2</sub>SnM are discussed using the results of *ab initio* pseudopotential total energy and band-structure calculations performed with a plane wave basis set using the conjugate gradients algorithm. The results characterize the lowest energy phase of NiSnM compounds, with a SnM rocksalt structure sublattice, as narrow gap semiconductors with indirect gaps near 0.5 eV, while the Ni<sub>2</sub>SnM compounds are described as normal metals. Two other atomic arrangements for NiSnM in the MgAgAs structure type result in energetically unfavorable compounds which are metallic. The gap formation in the lowest energy structure of NiSnZr and relative stability of the three atomic arrangements are investigated within a tight-binding framework and by considering the decompositions of each ternary compound into a binary substructure plus a third element sublattice. The stabilization of the lowest energy phase of NiSnZr is found to be mainly due to the relative stability of the SnZr rocksalt substructure, while the opening of the gap induced by the addition of the symmetry-breaking Ni sublattice makes a relatively minor contribution.

The results from the theoretical calculations for the NiSnM compounds are compared with the existing experimental data. From analysis of structural and chemical trends in the NiSnM compounds, CoVSn is predicted to be a new semiconducting intermetallic compound in the MgAgAs structure type. Preliminary first principles calculations suggest an indirect gap of 0.8 eV.  
61.50.Lt, 71.25.Pi, 71.25.Tn, 61.44.+p

## I. INTRODUCTION

Recent discoveries of unconventional electronic properties in multinary materials with complex crystal structures, such as quasicrystals and high  $T_c$  superconductors, have stimulated a growing demand for realistic theoretical studies of these systems. A full understanding of the interrelationships between composition, structure, and electronic properties of these complex systems requires a detailed analysis of individual materials at the microscopic level. While the quantum mechanical modeling of solids through first principles calculations has served as a very useful tool to obtain the microscopic information needed for structurally and chemically simple solids, there are practical problems associated with complex systems, especially with nonperiodic structures like quasicrystals. The challenge, therefore, is to identify simpler systems which can be fully studied with this theoretical tool, and yet shed light on issues that are relevant to the physics of more complex systems.

One issue that arises in the study of complex intermetallic systems is the formation of a (pseudo)gap in the electronic density of states (DOS) at the Fermi level and the relation of this feature to the stability of the particular structure. For quasicrystals, the presence of an (almost) universal suppression in the electronic DOS at the Fermi level has long been established both experimentally<sup>1</sup> and from first principles band-structure calculations for rational approximants.<sup>2</sup> It is widely believed that this particular feature of quasicrystals is related to their stability<sup>3</sup> based on an analogy to the Hume Rothery rule<sup>4</sup> for the stability of metallic alloys. The role of a pseudogap in structural stability has also been suggested by the experimental observation of very high resistivities in structurally well ordered stable quasicrystals.<sup>5,6</sup> Motivated by these observations, there has been recent interest in understanding the structural energetics, stability and transport properties of intermetallic compounds with small unit cells exhibiting a (pseudo)gap in their electronic spectrum. However, relatively few examples of such systems are known. CsAu is an extensively studied example<sup>7</sup> with a band gap of 2.6 eV. The electronic structure and transport properties of Al<sub>2</sub>Ru have recently been of considerable interest due to its structural simplicity and compositional

similarity to quasicrystals.<sup>6,8</sup> Another interesting class of intermetallic compounds with a pseudogap at the Fermi level is the skutterudite pnictides  $MA_3$  ( $M = \text{Co, Rh or Ir, and } A = \text{P, As or Sb}$ ). These compounds exhibit unusual transport properties making them likely candidates for advanced thermoelectric materials.<sup>9</sup> The identification of additional examples of intermetallic compounds with (pseudo)gaps is therefore a problem of both fundamental and technological interest.

A few years ago, the ternary intermetallic compounds  $NiSnM$  ( $M = \text{Ti, Zr, Hf}$ ) were reported to exhibit unusual transport and optical properties suggesting that they may have a gap at the Fermi level.<sup>10–13</sup> This observation establishes a possible new class of semiconducting intermetallics, which we have identified as good subjects for the theoretical study of band gap formation in intermetallics and its relation to structural stability.<sup>14</sup> These compounds crystallize in the  $MgAgAs$  structure and are related to the metallic Heusler compounds  $Ni_2SnM$  by the removal of an fcc Ni sublattice.<sup>15</sup> This simple crystal structure makes them quite suitable for a first principles approach<sup>16</sup> to the microscopic understanding of their unusual optical and electronic properties. While a complete understanding of these properties would require incorporating the effects of a high concentration of defects, calculations for the ideal structures should provide a useful starting point for further analysis. To understand the origin of the semiconducting gap in this system, one needs more than “simple” arguments. From a tight-binding analysis of the first principles bands and charge densities, both the  $pd$  hybridization on the  $SnM$  rocksalt substructure and the symmetry breaking due to the Ni sublattice are found to be crucial factors in gapping the electronic spectrum. Examination of total energies of ternary compounds and hypothetical binary substructures, calculated from first principles, allows us to conclude that the formation of the gap is not directly associated with structural stability in this system. Finally, the use of first principles information also assists us in identifying chemical trends for the prediction of related semiconducting intermetallics.

The rest of the paper is organized as follows. In Section II, we briefly discuss the technical details of the *ab initio* pseudopotential calculations for the  $NiSnM$  and  $Ni_2SnM$  compounds.

In Section III, we first examine their ground state structural properties and identify the correct atomic arrangement for the NiSnM compounds. This is followed by the results of band-structure and DOS calculations which characterize, within the local density approximation (LDA), the Ni<sub>2</sub>SnM compounds as normal metals, and the NiSnM compounds as narrow gap semiconductors with indirect gaps near 0.5 eV. In Section IV, we discuss these results in a tight-binding framework and by considering decompositions of the ternary structures into binary substructures plus a third element sublattice. Particular attention is given to the origin of the gap and structural stability of NiSnZr. We compare our results with available experimental measurements and, using the lessons from our analysis, we predict a new semiconducting intermetallic compound. Finally, our results are summarized in Section V.

## II. CALCULATIONAL PROCEDURE

For the calculation of band structures and total energies, we used the *ab initio* pseudopotential method with a plane wave basis set and the conjugate gradients algorithm.<sup>17</sup> The general technical issues that arise in the application of this method to intermetallic systems containing transition metals have been discussed in detail in Ref. 18. In this study, for Sn, Zr and Hf, we used the scalar-relativistic pseudopotentials of Bachelet, Hamann, and Schlüter<sup>19</sup> (BHS). For Ti and Ni, we constructed Hamann, Schlüter, and Chiang (HSC) pseudopotentials<sup>20</sup> for the *s* and *p* orbitals, and optimized pseudopotentials<sup>21</sup> (OPT) for the *d* orbitals. The exchange-correlation potential used in these calculations is the functional of Ceperley and Alder as parametrized by Perdew and Zunger.<sup>22</sup> Complete information concerning pseudopotential construction is given in Table I. These pseudopotentials were put into separable form using single or double projectors for each angular momentum (Table I) with the  $l = 0$  component as the local potential.<sup>23</sup> In all cases, the absence of ghost states and the transferability of pseudopotentials were checked by applying the ghost theorem of Gonze *et al.*<sup>24</sup> and comparing the logarithmic derivatives for these nonlocal pseudopotentials

with their all-electron values over a wide energy range.

All total energy and band-structure calculations were done on IBM RS/6000 workstations using the conjugate gradients program CASTEP 2.1,<sup>25</sup> slightly modified for metallic systems. The plane wave cutoff used in the calculations was determined by requiring the kinetic energy in the Fourier components of all atomic pseudo wave functions to be less than 1 mRy. This cutoff was set by the sharply peaked  $3d$  valence states of Ni to be 52 Ry, allowing us to perform accurate calculations with 2200-2800 plane waves depending on the size of the unit cell. Due to the metallic nature of some of the compounds investigated in this work, we used a Fermi-Dirac broadening<sup>26</sup> of 50 meV for  $\mathbf{k}$ -point sampling with Monkhorst-Pack<sup>27</sup> grids of  $q = 8$  and  $q = 10$ , resulting in 10 and 19  $\mathbf{k}$  points in the irreducible Brillouin zone (BZ), respectively. Lattice constants and bulk moduli were obtained by fitting to the Birch form, as described in Ref. 18.

The band-structure calculations for the NiSnM and Ni<sub>2</sub>SnM compounds were performed with self-consistent charge densities computed with a Monkhorst-Pack grid of  $q = 10$ . For DOS calculations, we first used this charge density to evaluate the band structure on a Monkhorst-Pack grid of  $q = 20$  (110  $\mathbf{k}$  points in the irreducible BZ), and interpolated the eigenvalues to a grid of  $\approx 225\,000$   $\mathbf{k}$  points in the irreducible fcc BZ using the interpolation scheme of Monkhorst and Pack<sup>27</sup> based on a global BZ fit. We then applied the Gilat-Raubenheimer method<sup>28</sup> to this fine mesh in the irreducible BZ. To check the accuracy of this interpolation, the calculated band structures along certain high symmetry lines were compared with the interpolated values, and the agreement was found to be very good within a few percent. Finally, for the band-structure plots and for use in the tight-binding analysis, symmetry labels along high symmetry lines were assigned using projection operators for the corresponding irreducible representations.

### III. RESULTS

The ternary crystal structures included in this study are the  $\text{BiF}_3$  structure for the  $\text{Ni}_2\text{SnM}$  compounds and the  $\text{MgAgAs}$  structure for the  $\text{NiSnM}$  compounds.<sup>15</sup> The crystal structure of  $\text{Ni}_2\text{SnM}$  (space group  $Fm\bar{3}m$ ), shown in Fig. 1(a), can be viewed as a rocksalt arrangement of Sn and M atoms with Ni atoms at the center of each cube of Sn-M atoms. The noncentrosymmetric crystal structure of  $\text{NiSnM}$  (space group  $F\bar{4}3m$ ), shown in Fig. 1(b), can be obtained from that of  $\text{Ni}_2\text{SnM}$  by eliminating one of the fcc Ni sublattices, resulting in tetrahedral coordination of the Sn and M atoms by Ni. We also considered two additional distinct  $\text{MgAgAs}$  type crystal structures obtained by interchanging the Ni, Sn and M sublattices. These three different crystal structures can be distinguished by identifying the doubly tetrahedrally coordinated element; the relevant coordination environments are shown in Fig. 2(a). We refer to these three structures as the  $\alpha$ ,  $\beta$ , and  $\gamma$  phases depending on whether Ni, Sn, or M is doubly tetrahedrally coordinated, respectively.<sup>16</sup>

First, we performed total energy calculations at several lattice constants for all six compounds  $\text{Ni}_2\text{SnM}$  and  $\text{NiSnM}$  (in the  $\alpha$  phase) to determine their ground state structural properties. The results are summarized in Table II. As seen from this table, the calculated equilibrium lattice constants are in very good agreement with experiment, with slight underestimates typical of the LDA. To our knowledge, no measurements of the bulk moduli for these compounds have been reported in the literature; the values in the table are therefore predictions for the bulk moduli of the  $\text{Ni}_2\text{SnM}$  and  $\text{NiSnM}$  compounds. We also performed total energy calculations for the  $\alpha$ ,  $\beta$ , and  $\gamma$  phases of  $\text{NiSnM}$ . Figure 2(b) shows the results of these calculations for  $M = \text{Zr}$ , and the  $\alpha$  phase is seen to be the lowest energy structure (2.28 and 2.85 eV/unit cell below the  $\beta$  and  $\gamma$  phases, respectively), consistent with reported structural determinations. The experimental lattice constant for the  $\text{NiSnZr}$  compound ( $6.11 \text{ \AA}$ )<sup>15</sup> is also closest to the LDA lattice constant of the  $\alpha$  phase. This calculation therefore unambiguously determines the crystal structure of the  $\text{NiSnM}$  compounds as the  $\alpha$  phase. The reasons behind the relative stability of the  $\alpha$ ,  $\beta$ , and  $\gamma$  phases will be discussed

in Section IV.

Next, we performed band-structure and DOS calculations for both  $\text{Ni}_2\text{SnM}$  and  $\text{NiSnM}$  compounds as a first step towards a microscopic understanding of their electronic structures. Figure 3 shows the calculated band structure along high symmetry lines of the fcc BZ for  $\text{Ni}_2\text{SnZr}$ . This exhibits normal metallic behavior with bands crossing the Fermi level along various directions, which results in a finite DOS at the Fermi level, as shown in Fig. 4. Very similar band structures and DOS were also obtained for  $\text{Ni}_2\text{SnTi}$  and  $\text{Ni}_2\text{SnHf}$ . On the other hand, band-structure calculations for the lowest energy structure of  $\text{NiSnM}$  (the  $\alpha$  phase) show that the Fermi level does not intersect any bands along the high symmetry directions, as can be seen in Fig. 5 for the case of  $\text{NiSnZr}$ . In fact, DOS calculations show that for these compounds there is a gap in the electronic DOS at the Fermi level (Fig. 6). For all three compounds, this is an indirect  $\Gamma \rightarrow X$  gap near 0.5 eV, while the direct gap, close to 1.1 eV, occurs at  $X$  (Table III). In contrast, band-structure calculations for the higher energy  $\beta$  and  $\gamma$  phases of  $\text{NiSnM}$  show metallic behavior (Fig. 7). Therefore, these LDA calculations characterize the  $\text{NiSnM}$  compounds in the  $\alpha$  phase as narrow gap semiconductors, while  $\text{Ni}_2\text{SnM}$  compounds and the  $\beta$  and  $\gamma$  phases of  $\text{NiSnM}$  are found to be normal metals.

#### IV. DISCUSSION

Using the results of first principles total energy and band-structure calculations, we can develop a physical understanding of the microscopic mechanisms in the formation of the band gap in the  $\alpha$  phase of  $\text{NiSnM}$ , and of the differences between these compounds and related systems, specifically the  $\beta$  and  $\gamma$  phases and  $\text{Ni}_2\text{SnM}$ . In Section IV A, we investigate the origin of the band gap in a tight-binding framework. In Section IV B, we consider the three phases of the ternary compounds  $\text{NiSnM}$  using the decompositions into a binary substructure plus a third element sublattice, and show that these decompositions can be quite useful in discussing the stability and electronic structures of ternary compounds. After a brief discussion of the differences between the metallic Heusler compounds  $\text{Ni}_2\text{SnM}$  and the



semiconducting NiSnM compounds in Section IV C, we examine the available experimental data on the NiSnM compounds from the point of view of our theoretical calculations in Section IV D. The relationships between band gap formation and structural stability in intermetallic compounds are considered in Section IV E, and the applicability of these ideas to the NiSnM compounds is examined. Finally, in Section IV F, we use the lessons gained from this analysis to predict a new semiconducting intermetallic compound. We note that for definiteness, the discussion in these sections is for  $M = \text{Zr}$ , though the overall features are the same for  $M = \text{Ti}$  and  $\text{Hf}$ .

### A. Origin of the band gap

Our tight-binding analysis begins with identification of the orbital characters of the valence and conduction bands. With a plane-wave basis set, this is accomplished by examining contour plots of the charge densities of individual states at various  $\mathbf{k}$  points. We first consider the bands well below the Fermi level. The lowest-lying band in Fig. 5 has predominantly Sn  $s$  orbital character, while the narrow bands above it have predominantly Ni  $d$  character. This seems to suggest a picture in which bands arising from the Sn  $s$ , Ni  $d$ , and either Sn  $p$  or  $t_{2g}$  type Zr  $d$  orbitals are fully occupied, forming a closed shell system with a gap to the next excited state. We therefore examined the triply degenerate  $\Gamma_{15}$  and the doubly degenerate  $X_5$  states just below the Fermi level, shown in Fig. 8(a). The charge density plots in the (110) plane show that the  $\Gamma_{15}$  states have mainly Zr  $d$  character [Fig. 8(c)], while the  $X_5$  states have mainly Sn  $p$  character [Fig. 8(e)]. This change in orbital character shows that the gap in NiSnM compounds cannot be due to a simple closed shell picture, since in that case we would expect the highest occupied band to be derived from either Sn  $p$  or Zr  $d$  orbitals.

A detailed analysis of band behavior is therefore needed to explain the formation of the gap. We focus on the bands  $\Gamma - \Delta - X$  as capturing the essential features of the gap mechanisms. Symmetry labels and orbital characters allow the separation of bands

into different subspaces which can be considered one at a time. We start with the highest occupied valence band  $\Delta_{3,4}$ . The doubly degenerate  $\Delta_{3,4}$  conduction band from  $\Gamma_{15}$  to  $X_5$  [Fig. 8(a)] has the same symmetry label, but complementary orbital character, changing from mainly Sn  $p$  at  $\Gamma$  [Fig. 8(b)] to mainly Zr  $d$  at  $X$  [Fig. 8(d)]. To describe this pair of bands, we use a tight-binding basis including the Sn  $p_x, p_y$ , and Zr  $d_{xz}, d_{yz}$  orbitals.<sup>29</sup> The behavior of these bands, shown with thick lines in Fig. 8(a), can be explained as arising from dispersive Zr  $d$  and Sn  $p$  type bands which hybridize along  $\Delta$  and anticross. The reason that this does not look like a familiar anticrossing of two bands (where the bands approach and then slightly repel each other) is that this  $pd$  hybridization is large and strongly  $\mathbf{k}$ -dependent, with the maximum value halfway along  $\Delta$ . Specifically, starting with nonzero interactions only for Sn-Sn and Zr-Zr nearest neighbors in the fcc lattice, the dispersion  $E_{x,y}(\alpha)$  for the Sn  $p_x$  and  $p_y$  orbitals is

$$E_{x,y}(\alpha) = \epsilon_p + 2(pp\sigma + pp\pi) + (2pp\sigma + 6pp\pi) \cos \pi\alpha \quad (4.1)$$

while the dispersion  $E_{xz,yz}(\alpha)$  for the Zr  $d_{xz}$  and  $d_{yz}$  orbitals is

$$E_{xz,yz}(\alpha) = \epsilon_d + 2(dd\pi + dd\delta) + (3dd\sigma + 2dd\pi + 3dd\delta) \cos \pi\alpha \quad (4.2)$$

where  $\alpha$  runs from 0 (at  $\Gamma$ ) to 1 (at  $X$ ). In these equations,  $\epsilon_p$  and  $\epsilon_d$  denote the onsite orbital energies of the  $p$  and  $d$  orbitals, respectively, and the definitions of the tight-binding parameters are as in Ref. 30. If the parameters are taken to have the usual approximate relative magnitudes and signs ( $dd\pi \approx -\frac{1}{2}dd\sigma$ ,  $dd\delta \approx 0$ ,  $dd\sigma < 0$ ,  $pp\pi \approx -\frac{1}{4}pp\sigma$ , and  $pp\sigma > 0$ ),<sup>30</sup> the  $p$  type bands disperse downward with a maximum at  $\Gamma$ , while the  $d$  type bands disperse upward with a minimum at  $\Gamma$ . With a suitable choice of the parameters, the two bands will cross. However, including a nearest neighbor Sn-Zr  $pd$  interaction will result in an anticrossing of these two bands, with a matrix element  $2pd\pi \sin \pi\alpha$  for this geometry, which is largest halfway along  $\Delta$ . This tight-binding parametrization reproduces the first principles dispersion and is consistent with the orbital character of the states obtained from charge density plots. This shows that the strong  $pd$  hybridization in the SnZr rocksalt

substructure is a necessary ingredient in the formation of the gap, for if it were zero, the  $\Gamma_{15}$  states below (above) the Fermi level would join with the  $X_5$  states above (below) the Fermi level resulting in a finite DOS at the Fermi level. However, this hybridization is not in itself sufficient for the gap formation in the ternary NiSnZr compound.

To complete the analysis of gap formation in the  $\alpha$  phase of NiSnZr, we must consider the conduction band minimum  $X_3$  [Fig. 8(a)], which has mainly Zr  $d_{xy}$  character. Since the valence band maximum  $\Gamma_{15}$  also has Zr  $d_{xy}$  character, an unhybridized Zr  $d_{xy}$  band, with  $\Delta_1$  symmetry, must anticross with  $\Delta_1$  bands derived from other orbitals for the gap to form. However, this anticrossing cannot be explained by considering *only* the SnZr substructure as in the case of  $\Delta_{3,4}$  bands. Due to the  $O_h$  symmetry of the rocksalt substructure, the matrix elements between the Zr  $d_{xy}$  band along  $\Delta$  and the bands derived from all other Zr  $d$  and Sn  $p$  orbitals vanish, resulting in zero anticrossing. For the gap to form, it is necessary to include the Ni  $d$  orbitals, lowering the symmetry of the system to  $T_d$ . Although the Ni  $d$  states lie well below the Fermi level, the Ni  $d_{xy}$  and  $d_{3z^2-r^2}$  orbitals mediate an *indirect* interaction between the Zr  $d_{xy}$  band and the bands derived from the Zr  $d_{3z^2-r^2}$  and Sn  $p_z$  orbitals. These interactions lead to a nonzero anticrossing of these bands, opening the gap at the Fermi level. Therefore, the symmetry breaking produced by the third element (Ni) sublattice is the essential additional ingredient in the formation of the gap.

## B. Ternary compounds from binary substructures

The analysis of the previous section showed that the states near the Fermi level in the  $\alpha$  phase of NiSnZr are dominated by the atomic orbitals of the SnZr rocksalt substructure. This suggests an approach to the analysis of the electronic structure and stability of the ternary compound through the identification of a key binary substructure. In this approach, the essential features of electronic structure and stability should already be evident in the binary substructure, while addition of the third element sublattice leads to recognizable modifications such as (i) introduction of extra orbitals hybridizing with the orbitals of the

binary substructure, (ii) change in the symmetry of the crystal structure, and (iii) charge transfer between the binary substructure and the third element sublattice, and other changes in the self-consistent charge density.

We apply this approach to NiSnZr by computing the total energies and band structures for the binary substructures appearing in the decomposition of the  $\alpha$ ,  $\beta$  and  $\gamma$  phases. There are six distinct substructures: SnZr, NiZr and NiSn in the rocksalt ( $B1$ ) and zincblende ( $B3$ ) structures. The total energies of these six substructures at the lattice constant of the  $\alpha$  phase, with lists of the corresponding NiSnZr phases, are given in Table IV. For each of the three binary compositions, the lower energy structure (between  $B1$  and  $B3$ ) is the one contained in the decomposition of the  $\alpha$  phase. However, consideration of the magnitudes of the  $B1$ - $B3$  energy differences singles out the decomposition containing the SnZr substructure. The  $B1$  structure of SnZr is 2.03 eV lower in energy than the  $B3$  structure. This value is quite close to the energy difference between the  $\alpha$  phase, containing the  $B1$  SnZr substructure, and the  $\beta$  and  $\gamma$  phases, which contain the  $B3$  SnZr substructure (2.28 eV and 2.85 eV, respectively). In contrast, the  $B1$ - $B3$  energy differences for NiZr and NiSn are too small (0.26 eV and 0.23 eV per unit cell, respectively) to be relevant to the stabilization of the  $\alpha$  phase relative to the  $\beta$  and  $\gamma$  phases. Therefore, the low energy of the NiSnZr compound in the  $\alpha$  phase can be mainly attributed to the stability of the SnZr  $B1$  substructure.

There also appear to be useful relationships between the band structures of the ternary compounds and those of binary substructures. For example, the  $\alpha$  phase of NiSnZr, where the SnZr substructure is rocksalt, has a gap while the  $\beta$  and  $\gamma$  phases, with SnZr in a zincblende arrangement, are both metallic. We investigate these relationships in more detail by examining the band structures of the six substructures (Fig. 9) and comparing them with the band structures of the ternary  $\alpha$  [Fig. 8(a)],  $\beta$  [Fig. 7(a)] and  $\gamma$  [Fig. 7(b)] phases. In the  $B3$  phases of NiSn and NiZr, the crystal field splittings of the Ni and Zr  $d$  states at  $\Gamma$  are noticeably larger than in the  $B1$  phases. The reason is that the point symmetry is lowered from  $O_h$  in the  $B1$  structure to  $T_d$  in the  $B3$  structure, resulting in a mutual repulsion of  $t_{2g}$  type  $d$  and  $p$  orbitals in the latter. Comparison of the  $B1$  with the  $B3$  band structures for

the three compositions shows a striking difference between NiZr and NiSn, on the one hand, and SnZr, on the other hand, in the position of the Fermi level and dispersion of the nearby bands. The very small change in the position of the Fermi levels for the two structures of NiZr and NiSn is not surprising, because the Ni  $d$  orbitals are rather low-lying, and do not substantially affect states around the Fermi level in these compounds. In contrast, the arrangement of the bands and position of the Fermi level changes noticeably from SnZr  $B1$  to SnZr  $B3$ . This occurs because Zr  $d$  and Sn  $p$  orbitals are partially occupied orbitals involved in bonding, making the band dispersions and the positions of the Fermi level quite sensitive to the atomic arrangement.

We can also compare the band structures of the three phases of the ternary compound with the band structures of the  $B1$  and  $B3$  structures of SnZr that appear in their decompositions. For example, comparison of Fig. 8(a) and the band structure of SnZr in the  $B1$  structure (Fig. 9) shows that the low-lying Sn  $s$  band, the conduction bands well above the Fermi level, and the bands arising from the Sn  $p_x, p_y$  and Zr  $d_{xz}, d_{yz}$  hybridizations (labelled by  $\Delta_5$  in Fig. 9) look quite similar to those in Fig. 8(a). On the other hand, the  $\Delta_1$  band in Fig. 9, arising from the doubly degenerate  $\Gamma_{12}$  state and ending up as the  $X'_2$  state at  $X$  is substantially modified by the introduction of the Ni sublattice. In the ternary compound, this band anticrosses due to the presence of Ni  $d$  orbitals and reduced point group symmetry. Closer examination shows that the introduction of the Ni  $d$  orbital greatly increases the crystal field splitting of the Zr  $d$  states at  $\Gamma$ , with the Fermi level in the  $\alpha$  phase of NiSnZr placed just inside this splitting. Thus, within the substructure decomposition approach, we can account for the formation of the gap. The band structure of NiSnZr in the  $\gamma$  phase [Fig. 7(b)] also has similarities with the band structure of SnZr in the  $B3$  structure (Fig. 9). Since the Sn  $p$ -Zr  $d$  interaction pushes the  $t_{2g}$  type Zr  $d$  states down in energy in the  $B3$  structure, the introduction of Ni  $d$  orbitals results in the formation of a  $d$ -band complex below the Fermi level, while the downward dispersing bands well above the Fermi level are not substantially affected by this. On the other hand, the relationship between the band structure of the  $\beta$  phase of NiSnZr [Fig. 7(a)] with the band structure of its  $B3$  SnZr

substructure is much more complicated, because introducing the Ni  $d$  orbitals changes the mixing of the  $p$  and  $d$  orbitals to a greater extent due to double tetrahedral coordination of Sn. In this case, it is not possible to treat the effects of the Ni  $d$  orbitals perturbatively.

### C. Comparison of Ni<sub>2</sub>SnM with NiSnM

The Ni<sub>2</sub>SnM compounds can be produced from the  $\alpha$  phase of NiSnM by adding a Ni sublattice, which changes the system from a narrow gap semiconductor to a metal. The effect of the additional sublattice responsible for this change in electronic structure is the raising of the noncentrosymmetric  $T_d$  symmetry to the centrosymmetric  $O_h$  point group symmetry, with consequent changes in the symmetry properties of atomic-orbital Bloch functions. In particular, if  $\phi$  denotes any of the five  $d$  or  $s$  orbitals of Ni, the functions that transform according to the irreducible representations of the point group of any high symmetry point in the BZ have the form  $\frac{1}{\sqrt{2}}(\phi^{(1)} \mp \phi^{(2)})$ , where  $\phi^{(i)}$  ( $i = 1, 2$ ) denotes the  $\phi$  orbital of the  $i^{\text{th}}$  Ni atom in the unit cell. Also, any orbital that transforms according to  $\Delta_1$  ( $X_3$ ) in the noncentrosymmetric compound transforms in Ni<sub>2</sub>SnM according to either  $\Delta_1$  or  $\Delta'_2$  ( $X_4$  or  $X'_2$ ). Therefore, the  $\Delta_1$  and  $\Delta'_2$  bands near the Fermi level (Fig. 3) do not anticross as they do in NiSnM, where they both carry the  $\Delta_1$  label. As a result, the  $\Delta_1$  band cuts the Fermi level, producing the metallic behavior. Finally, in our calculations we do not see any evidence of a vacancy band<sup>13</sup> proposed to explain the experimental data for NiSnM. This is not too surprising for the perfectly clean samples on which our calculations were based, because unlike the case of heavy doped semiconductors, the vacancies in this system are very well ordered (in an fcc lattice) and have a high concentration.

### D. Comparison with experiment

What light do these calculations shed on the experimentally observed electronic and optical properties of the NiSnM compounds? First of all, the very high low-temperature

resistivities with a simple exponential temperature dependence observed in the NiSnM compounds are consistent with the appearance of a semiconducting gap in the calculated band structures. However, specific heat measurements show a small but finite DOS at the Fermi level.<sup>13</sup> Furthermore, the calculated gaps are all near 0.5 eV. These are more than twice as large as the gap parameters 0.12, 0.19, and 0.22 eV for Ti-, Zr-, and Hf-based compounds, respectively, extracted from resistivity measurements<sup>12</sup> and features in the optical reflectivity  $R(\omega)$ .<sup>11</sup> While LDA errors (either underestimates or overestimates) in the values of the band gaps are expected, a more serious problem which could give rise to these discrepancies is poor sample quality, particularly substitutional disorder. In NiSnZr, there is direct evidence from x-ray diffraction for Sn-Zr substitutional disorder at the 10-30% level.<sup>10</sup> The degree of substitutional disorder seems to be correlated with changes in the electronic properties. One example of this is that the DOS at the Fermi level appears to decrease as the degree of disorder decreases. In particular, the zero temperature resistivity increases dramatically upon annealing the samples.<sup>10</sup> Also, the DOS at the Fermi level from specific heat measurements<sup>13</sup> is lowest for the Ti-based compound, which has the smallest disorder in the position of the Ti and Sn atoms, indicating that a complete gap may be expected to open in a very clean sample. To improve our understanding of the effect of the Sn-Zr substitutional disorder on the size of the gap, we performed total energy and band-structure calculations for  $\text{Ni}(\text{Sn}_{1-x}\text{Zr}_x)(\text{Sn}_x\text{Zr}_{1-x})$  for a few values of  $x$  between 0 and 0.5 in the virtual crystal approximation. At around  $x = 0.15$ , the gap closes to form a semimetal, with the valence band maximum (conduction band minimum) moving up (down) in energy and touching the Fermi level. Therefore, to achieve experimental gap values comparable to those calculated for the ideal crystals, special attention to sample preparation is needed. In such well-ordered samples, reflectivity measurements would have to be extended to higher frequencies than those used in previous studies (in Ref. 11  $\omega < 5000 \text{ cm}^{-1}$ ) to see the onset of absorption.

### E. Band gap and structural stability

Direct relations between the formation of a (pseudo)gap and the stability of the structure have been proposed in several contexts, including the Hume Rothery rule,<sup>3,4</sup> Jahn-Teller effects in molecules,<sup>31</sup> and the “coloring” patterns of atoms over the sites of a given lattice.<sup>32</sup> If the formation of a gap in the DOS is an important factor in the structural stability of intermetallic compounds, the expectation is that semiconducting intermetallics would be fairly common, while, as we have already discussed, they are quite rare. Therefore, it is useful to examine this issue in the present case.

For NiSnM compounds in their  $\alpha$ ,  $\beta$ , and  $\gamma$  phases, it is true that the structure with the gap has the lowest energy, and there is a correlation between the DOS at the Fermi level and the structural energies of the three phases. However, the present calculations suggest that the formation of the gap is not directly responsible for the structural stability. Instead, the stability can be understood from the substructure decomposition approach. As discussed in Sec. IV B, the energy of the SnZr *B1* structure is 2.03 eV per unit cell lower than that of the *B3* structure. From Fig. 9, it is clear that neither the *B1* nor the *B3* SnZr structures have a gap. The ternary phases are obtained by incorporating the Ni sublattice into the binary SnZr substructures. This incorporation produces a gap in the  $\alpha$  phase, as a result of symmetry breaking, but leads to only a small change in the relative energy (from 2.03 eV per unit cell to energy differences of 2.28 eV and 2.85 eV per unit cell between the  $\alpha$  and the  $\beta$  and  $\gamma$  phases, respectively). Therefore, the stabilization of the lowest energy phase is primarily due to the relative stability of the binary SnZr *B1* substructure, while the contribution to stabilization associated with the incorporation of the third element (Ni) sublattice, which results in the formation of the gap, is relatively minor. This conclusion is not inconsistent with the relations between gap formation and stability observed elsewhere. In the Hume-Rothery rule, a gap in the DOS establishes the limit of stability of a particular alloy structure as a function of electron count, rather than an enhanced stability specifically of the semiconducting phase. In the Jahn-Teller and



coloring analyses, the correlation between structural stability and gap formation is identified in classes of structures which are otherwise extremely similar (related by small structural relaxations in the Jahn-Teller case and possessing identical nearest neighbor environments for the cations in the coloring problem). However, in the NiSnM compounds, the  $\alpha$ ,  $\beta$  and  $\gamma$  phases are related by sublattice interchanges, not small displacements, resulting in different nearest neighbor environments in each phase. It is therefore reasonable that the substructure decomposition approach, with the identification of the low-energy rocksalt SnZr substructure, should be a more useful indicator of structural stability than gap formation for these compounds.

#### F. Considerations for new semiconducting intermetallics

From these results, the simple chemical and structural trends in gap formation can be identified and used to assist in the prediction of new semiconducting intermetallics. We have already seen that a closed shell rule with 18 electrons is too simple. The ternary nature of the compounds, particularly the electronegativity difference between the constituents of the rocksalt substructure, and the structural arrangement, particularly the double tetrahedral coordination of the late transition metal, seem to be important factors, since the hypothetical compounds NiSn<sub>2</sub> and NiZr<sub>2</sub>, and the  $\beta$  and  $\gamma$  phases of NiSnM compounds are metallic.<sup>33</sup> On the other hand, the empirical rule that the total number of  $d$  electrons from the two transition metals in their ground states should be 10 works for the NiSnM compounds as well as for the compounds formed by the column substitutions of Ni with Pd and Pt.<sup>12</sup> It is also necessary that the transition metal that is doubly tetrahedrally coordinated should have a significantly larger number of  $d$  electrons in the atomic ground state, so that the bands originating from these  $d$  orbitals will lie deep below the Fermi level, and not destroy the  $pd$  hybridizations by mixing significantly with the  $d$  orbitals of the other transition metal. CoVSn in the MgAgAs structure with Co doubly tetrahedrally coordinated by Sn and V satisfies these rules. First-principles band structure calculations confirm that CoVSn has an

$L \rightarrow X$  gap of 0.8 eV at the Fermi level (Fig. 10). This compound is not reported to exist in the intermetallic compound database. However, there is a good chance that this might be a stable compound based on the analogy with the  $\alpha$  phase of NiSnM compounds. Therefore, we predict that if this compound can successfully be prepared in this structure, it will be a semiconducting intermetallic.

## V. CONCLUSIONS

In this paper, we used the pseudopotential total energy method to investigate the stability and electronic structure of the ternary intermetallic compounds NiSnM ( $M = \text{Ti, Zr, Hf}$ ). Our calculations revealed an indirect semiconducting gap near 0.5 eV for all three compounds in the lowest energy  $\alpha$  phase, while the inversion symmetric  $\text{Ni}_2\text{SnM}$  compounds and the higher energy  $\beta$  and  $\gamma$  phases of NiSnM were found to be metallic. From a tight-binding analysis of the first-principles bands and charge densities, both the  $pd$  hybridization on the SnZr rocksalt substructure and the symmetry breaking due to the Ni sublattice were found to be crucial factors in gapping the electronic spectrum of  $\alpha$ -NiSnZr. By considering all binary substructures which appear in the decomposition of the three phases of NiSnZr, we concluded that the stabilization of the lowest energy  $\alpha$  phase is primarily due to the relative stability of the binary SnZr  $B1$  substructure, while the contribution to stabilization associated with the incorporation of the third element (Ni) sublattice, which results in the formation of the gap, is relatively minor. Analysis of the band structures for the narrow gap semiconductor NiSnZr and the metallic  $\text{Ni}_2\text{SnZr}$  showed that the raising of the point group symmetry from the noncentrosymmetric  $T_d$  to the centrosymmetric  $O_h$  group by the addition of the Ni sublattice is responsible for this difference in the electronic properties. Our theoretical findings are consistent with experimental observations, if poor sample quality and substitutional disorder in the samples are taken into account. Finally, we predicted that the ternary compound CoVSn in the MgAgAs structure with an SnV rocksalt substructure will form a semiconducting intermetallic, if it can be prepared successfully in this structure.

## ACKNOWLEDGMENTS

We would like to thank J. C. Phillips, L. F. Mattheiss, W. A. Harrison, J. K. Burdett, J. Rodgers, U. V. Waghmare, and R. B. Phillips for many useful discussions. We would also like to thank M. C. Payne for the use of CASTEP 2.1. This work was supported by NSF Grant No. DMR-9057442. In addition, K. M. R acknowledges the support of the Clare Boothe Luce Fund and the Alfred P. Sloan Foundation.

## REFERENCES

- <sup>1</sup> S. J. Poon, Adv. Phys. **41**, 303 (1992); *Proceedings of the Fourth International Conference on Quasicrystals*, edited by K. F. Kelton, P. C. Gibbons, and A. I. Goldman, J. Non-Cryst. Solids **153 & 154**, (1993).
- <sup>2</sup> T. Fujiwara and T. Yokokawa, Phys. Rev. Lett. **66**, 333 (1991); J. Hafner and M. Krajci, *ibid.* **68**, 2321 (1992).
- <sup>3</sup> P. A. Bancel and P. A. Heiney, Phys. Rev. B **33**, 7917 (1986); V. G. Vaks, V. V. Kamyshenko, and G. D. Samolyuk; Phys. Lett. A **132**, 131 (1988); J. Friedel, Helv. Phys. Acta **61**, 538 (1988); C. Janot and M. de Boissieu, Phys. Rev. Lett **72**, 674 (1994).
- <sup>4</sup> See, e.g., N. F. Mott and H. Jones, *The Theory of the Properties of Metals and Alloys* (Oxford University Press, London 1936); A. R. Williams and D. Weaire, J. Phys. C **3**, 387 (1970); D. Stroud and N. W. Ashcroft, J. Phys. F **1**, 113 (1971).
- <sup>5</sup> T. Matsuda *et al.*, J. Phys. Condens. Matter **1**, 4087 (1989); T. Klein *et al.*, Europhys. Lett. **13**, 129 (1990); B. D. Biggs, S. J. Poon, and N. R. Munirathman, Phys. Rev. Lett. **65**, 2700 (1990); P. Lanco *et al.*, Europhys. Lett. **18**, 227 (1992); F. S. Pierce, S. J. Poon, and Q. Guo, Science **261**, 737 (1993).
- <sup>6</sup> F. S. Pierce *et al.*, Phys. Rev. Lett. **70**, 3919 (1993); D. N. Basov *et al.*, *ibid.* **73**, 1865 (1994).
- <sup>7</sup> C. Koenig, N. E. Christensen, and J. Kollar, Phys. Rev. B **29**, 6481 (1984), and references therein.
- <sup>8</sup> D. N. Manh *et al.*, Solid State Comm. **82**, 329 (1992).
- <sup>9</sup> D. J. Singh and W. E. Pickett, Phys. Rev. B **50**, 11235 (1994).
- <sup>10</sup> F. G. Aliev *et al.*, Sov. J. Low Temp. Phys. **13**, 281 (1987); F. G. Aliev *et al.*, JETP Lett. **45**, 684 (1987).

- <sup>11</sup> F. G. Aliev *et al.*, JETP Lett. **47**, 184 (1988).
- <sup>12</sup> F. G. Aliev *et al.*, Z. Phys. B **75**, 167 (1989).
- <sup>13</sup> F. G. Aliev *et al.*, Z. Phys. B **80**, 353 (1990).
- <sup>14</sup> S. Ögüt and K. M. Rabe, to be published in Turk. J. Phys. (1995).
- <sup>15</sup> P. Villars and L. D. Calvert, *Pearson's Handbook of Crystallographic Data for Intermetallic Phases*, (American Society of Metals, Metals Park, OH, 1985).
- <sup>16</sup> Su-H. Wei and A. Zunger, Phys. Rev. Lett. **56**, 528 (1986).
- <sup>17</sup> M. C. Payne, M. P. Teter, D. C. Allan, T. A. Arias, and J. D. Joannopoulos, Rev. Mod. Phys. **64**, 1045 (1992).
- <sup>18</sup> S. Ögüt and K. M. Rabe, Phys. Rev. B **50**, 2075 (1994).
- <sup>19</sup> G. B. Bachelet, D. R. Hamann, and M. Schlüter, Phys. Rev. B **26**, 4199 (1982).
- <sup>20</sup> D. R. Hamann, M. Schlüter, and C. Chiang, Phys. Rev. Lett. **43**, 1494 (1979).
- <sup>21</sup> A. M. Rappe, K. M. Rabe, E. Kaxiras, and J. D. Joannopoulos, Phys. Rev. B **41**, 1227 (1990).
- <sup>22</sup> D. M. Ceperley and B. J. Alder, Phys. Rev. Lett. **45**, 566 (1980); J. P. Perdew and A. Zunger, Phys. Rev. B **23**, 5048 (1981).
- <sup>23</sup> L. Kleinman and D. M. Bylander, Phys. Rev. Lett. **48**, 1425 (1982); P. E. Blöchl, Phys. Rev. B, **41** 5414 (1990).
- <sup>24</sup> X. Gonze, P. Käckell, and M. Scheffler, Phys. Rev B **41**, 12264 (1990).
- <sup>25</sup> M. C. Payne, X. Weng, B. Hammer, G. Francis, I. Stich, U. Bertram, A. de Vita, J. S. Lin, V. Milman, and A. Qteish (unpublished).
- <sup>26</sup> M. J. Gillan, J. Phys. Condens. Matter **1**, 689 (1989).

<sup>27</sup> H. J. Monkhorst and J. D. Pack, Phys. Rev. B **13**, 5188 (1976).

<sup>28</sup> G. Gilat and L. C. Raubenheimer, Phys. Rev **144**, 390 (1966).

<sup>29</sup> It should be noted that in this approximate analysis, the Ni  $d_{xz}$  and  $d_{yz}$  orbitals which also transform according to the same irreducible representations along  $\Delta$  are neglected. This is quite safe, because these orbitals are rather deep-lying, and do not have an appreciable mixing with either of the bands in the vicinity of the Fermi level, as can be checked from charge density plots. We also note that the functions that transform according to the  $\Delta_3$  and  $\Delta_4$  irreducible representations are not actually the Bloch sums of  $p_x$ ,  $p_y$ ,  $d_{xz}$ , and  $d_{yz}$  orbitals, but rather the linear combinations  $\frac{1}{\sqrt{2}}(p_x \mp p_y)$  and  $\frac{1}{\sqrt{2}}(d_{xz} \mp d_{yz})$ . However, this does not change the dispersion relations given by Eqs. (4.1) and (4.2), nor does it change the form of the coupling between the Sn  $p$  and Zr  $d$  orbitals.

<sup>30</sup> W. A. Harrison, *Electronic Structure and the Properties of Solids*, (W. H. Freeman and Company, San Fransisco, 1980).

<sup>31</sup> L. S. Bartell, J. Chem. Educ. **45**, 754 (1968); R. Hoffmann, J. Chem. Soc., Chem. Commun. 240 (1969).

<sup>32</sup> J. K. Burdett, S. Lee, and T. J. McLarnan, J. Amer. Chem. Soc. **107**, 3038 (1985); J. K. Burdett, B. A. Coddens, and G. V. Kulkarni, Inorg. Chem. **27**, 3259 (1988).

<sup>33</sup> We should note that since the band overlap in the  $\beta$  phase is quite small, self-energy corrections may also make this phase semiconducting, though with a much smaller band gap compared to the  $\alpha$  phase.

## FIGURES

FIG. 1. The crystal structures of (a)  $\text{Ni}_2\text{SnM}$ ; (b)  $\text{NiSnM}$  compounds.

FIG. 2. (a) Three possible coordination environments corresponding to the  $\alpha$  (bottom),  $\beta$  (middle), and  $\gamma$  (top) phases of  $\text{NiSnM}$ ; (b) Total energy versus the lattice constant for the  $\alpha$ ,  $\beta$ , and  $\gamma$  phases of  $\text{NiSnZr}$ . The energies shown in this graph are with respect to the minimum energy corresponding to the LDA lattice constant of the  $\alpha$  phase.

FIG. 3. The energy bands of  $\text{Ni}_2\text{SnZr}$  along the high symmetry lines of the fcc Brillouin zone. The calculations were performed at the experimental lattice constant of  $6.27 \text{ \AA}$ . The dotted line is the Fermi level. The symmetry labels are shown only for states that are discussed in Section IV C.

FIG. 4. Electronic density of states for  $\text{Ni}_2\text{SnZr}$ . The calculations were performed at the experimental lattice constant of  $6.27 \text{ \AA}$ . The dotted line is the the Fermi level.

FIG. 5. The energy bands of  $\text{NiSnZr}$  along the high symmetry lines of the fcc Brillouin zone. The calculations were performed at the experimental lattice constant of  $6.11 \text{ \AA}$ . The dotted line is the Fermi level.

FIG. 6. Electronic density of states for  $\text{NiSnZr}$ . The calculations were performed at the experimental lattice constant of  $6.11 \text{ \AA}$ . The dotted line is the the Fermi level.

FIG. 7. The energy bands of  $\text{NiSnZr}$  in the (a)  $\beta$ ; (b)  $\gamma$  phase along  $\Delta$ . The calculations were performed at a lattice constant of  $6.11 \text{ \AA}$ . The dotted lines represent the position of the Fermi level.

FIG. 8. (a) The energy bands of  $\text{NiSnZr}$  along  $\Delta$ . The thick curves are the doubly degenerate (due to time reversal symmetry)  $\Delta_{3,4}$  bands mentioned in the text; (b)-(c) Charge density contour plots for the triply degenerate  $\Gamma_{15}$  states; (d)-(e) Charge density contour plots for the doubly degenerate  $X_5$  states. The circles filled with  $\times$  marks and thick dots represent the positions of the Sn and Zr atoms, respectively.

FIG. 9. The energy bands for the SnZr, NiZr, and NiSn binary compounds in the  $B1$  and  $B3$  structures along  $\Delta$ . All calculations were performed at a fixed lattice constant of  $6.11 \text{ \AA}$ . The dotted lines represent the position of the Fermi level.

FIG. 10. Band structure of CoVSn in the MgAgAs structure along  $L - \Lambda - \Gamma - \Delta - X$ . The dotted line is the Fermi level. The calculations were performed at a lattice constant of  $5.9 \text{ \AA}$ .



TABLES

TABLE I. Parameters and methods used in the construction of the pseudopotentials. For OPT,  $q_c$  and N in the last two columns refer to the cutoff above which the kinetic energy is minimized and the number of Bessel functions used to expand the pseudo wave functions, respectively.<sup>21</sup>

Element	Configuration	Type	Projector <sup>a</sup>	$r_c$ (a.u)	$q_c$ (Ry)	N
Ni	4s <sup>0.75</sup> 4p <sup>0.25</sup> 3d <sup>8</sup>	s, p HSC	p, single	1.2, 1.2		
		d, OPT	d, single	2.0	7.15	10
Ti	4s <sup>0.75</sup> 4p <sup>0.25</sup> 3d <sup>2</sup>	s, p HSC	p, single	1.3, 1.4		
		d, OPT	d, single	1.9	6.80	4
Sn	5s <sup>1</sup> 5p <sup>0.5</sup> 5d <sup>0.5</sup>	BHS	p, double			
			d, double			
Zr	5s <sup>0.75</sup> 5p <sup>0.25</sup> 4d <sup>2</sup>	BHS	p, double			
			d, double			
Hf	6s <sup>0.75</sup> 6p <sup>0.25</sup> 5d <sup>2</sup>	BHS	p, single			
			d, double			

<sup>a</sup>The  $l = 0$  component was chosen as the local pseudopotential.

TABLE II. The experimental and calculated structural properties of the Ni<sub>2</sub>SnM and NiSnM compounds.

Compound	$a_{exp.}$ (Å) <sup>a</sup>	$a_{calc.}$ (Å)	B (Mbar) <sup>b</sup>
Ni <sub>2</sub> SnTi	6.09	6.00	1.64 (2.14)
Ni <sub>2</sub> SnZr	6.27	6.24	1.49 (1.59)
Ni <sub>2</sub> SnHf	6.24	6.13	1.36 (1.72)
NiSnTi	5.92	5.814	1.11 (1.43)
NiSnZr	6.11	6.07	1.19 (1.29)
NiSnHf	6.066	5.95	1.10 (1.41)

<sup>a</sup>From Ref. 15 and Fig. 5 in Ref. 12.

<sup>b</sup>The values in parentheses are the bulk moduli calculated at the LDA lattice constant.

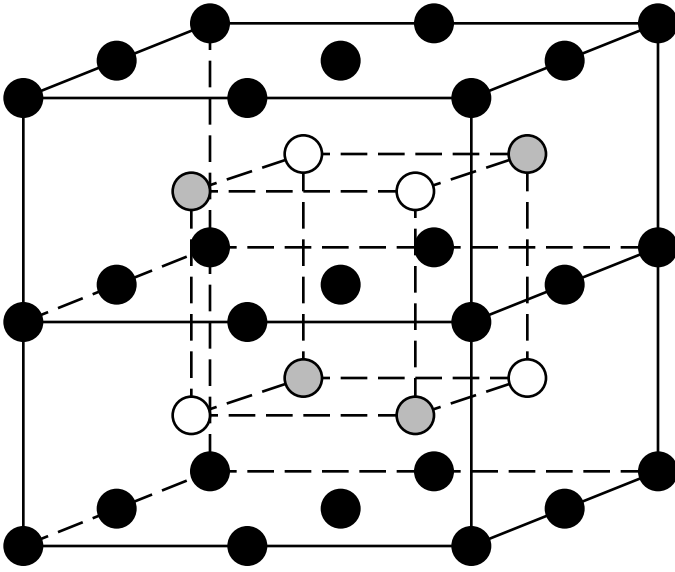
TABLE III. LDA band gaps for NiSnM compounds. The indirect gap occurs along  $\Gamma$  to  $X$ , while the direct gap occurs at  $X$ .

Compound	Indirect gap (eV)	Direct gap (eV)
NiSnTi	0.51	1.20
NiSnZr	0.51	1.05
NiSnHf	0.48	1.16

TABLE IV. Total energies for six different binary compounds which appear in the decomposition of the  $\alpha$ ,  $\beta$ , and  $\gamma$  phases of NiSnZr into  $B1$  and  $B3$  structures. The Greek letters in the parentheses under the second column give the phase of NiSnZr which will be obtained by the addition of the third type of element into either the tetrahedral or the octahedral hole of the fcc unit cell. All calculations were performed at a fixed lattice constant of 6.11 Å.

Compound	Structure	Total Energy (eV)
SnZr	$B1$ ( $\alpha$ )	-180.200
SnZr	$B3$ ( $\beta, \gamma$ )	-178.172
NiZr	$B1$ ( $\beta$ )	-997.115
NiZr	$B3$ ( $\alpha, \gamma$ )	-997.375
NiSn	$B1$ ( $\gamma$ )	-1011.445
NiSn	$B3$ ( $\alpha, \beta$ )	-1011.671

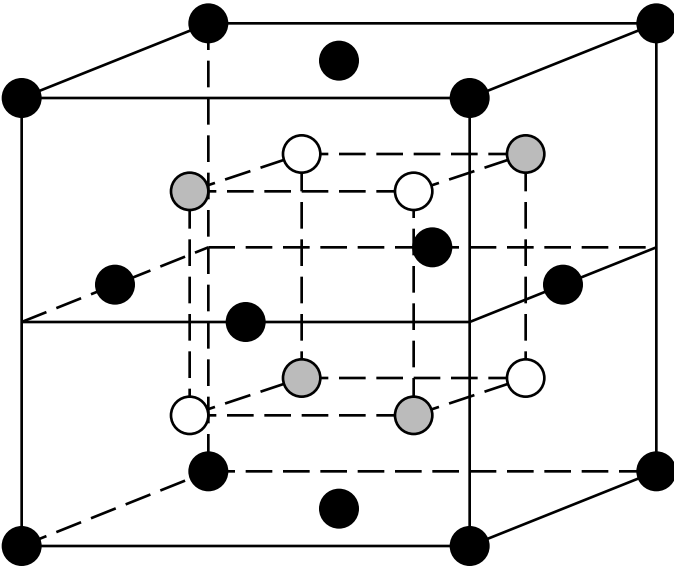
(a)



● Ni

● Sn

(b)



○ M

